J Mater Sci: Mater Electron
DOI 10.1007/s10854-016-6125-6

Dielectric properties, complex impedance and electrical conductivity of Fe_2TiO_5 nanopowder compacts and bulk samples at elevated temperatures

M. V. Nikolic[1] · D. L. Sekulic[2] · Z. Z. Vasiljevic[3] · M. D. Lukovic[1] · V. B. Pavlovic[3] · O. S. Aleksic[1]

Received: 23 September 2016 / Accepted: 21 November 2016

Abstract In this work we have investigated changes in dielectric properties, electrical conductivity and complex impedance of Fe_2TiO_5 nanopowder compacts and bulk samples as a function of elevated temperature (room to 423 K compacts, to 443 K bulk samples), frequency (100 Hz–1 MHz) and composition (starting molar ratio of Fe_2O_3 and TiO_2 1:1—PSB11 and 1:1.5—PSB115). XRD, SEM and TEM analysis of PSB11 and PSB115 powders obtained by a simple solid state process from starting hematite and anatase nanopowders confirmed the formation of nanostructured orthorhombic pseudobrookite with small amounts of excess hematite and rutile. The dielectric constant decreased with frequency and temperature for both compacts and bulk samples. Higher values were determined for bulk samples also reflecting the influence of sample composition. Change in the dielectric loss also reflected the influence of sample composition showing one maximum at high frequencies for compacts, and two maxima at room temperature for bulk samples. Complex impedance was analyzed using equivalent circuits and showed in the case of compacts the influence of both grain and grain boundary components, while in the case of bulk samples the dominant influence of grain boundaries. The temperature dependence of the determined grain and grain boundary resistance for compacts and grain boundary resistance for bulk samples was analyzed using the adiabatic small polaron hopping model enabling determination of activation energies for conduction, while the temperature dependence of relaxation times enabled determination of activation energies for relaxation. Changes in electrical conductivity for compacts and bulk samples followed Jonscher's power law. The change of the determined frequency constant with temperature showed that at elevated temperatures the quantum mechanical-tunneling model for the case of small polaron hopping explains the conduction mechanism occurring in both compacts and bulk samples.

1 Introduction

Pseudobrookite iron titanate (Fe_2TiO_5) is a n-type narrow bandgap semiconductor (2.2 eV) with a valence band edge surpassing water oxidation and a conduction band gap minimum near the energy level of TiO_2 [1]. It is has been the focus of recent research as a promising photocatalyst [2, 3]. Pseudobrookite has a wide range of potential applications including photoanode for water-splitting [4, 5], ceramic pigments [6], hydrogen generation [7], Li-ion battery anode [8] or gas sensor [9, 10]. Pseudobrookite exhibits anisotropic magnetic spin glass behavior [11, 12] and has two successive glassy freezing temperatures, transverse at 9 K and longitudinal at 55 K. Multiglass properties and magnetoelectric coupling of a polycrystalline sample of Fe_2TiO_5 were recently analyzed by Sharma et al. [13].

Gas sensors made of polycrystalline metal oxide semiconductors are greatly influenced by microstructural features, such as the grain size, defects, connectivity between particles. They generally operate at elevated temperatures that depend on the detection gas and used metal oxide.

✉ M. V. Nikolic
mariav@rcub.bg.ac.rs

[1] Institute for Multidisciplinary Research, University of Belgrade, Kneza Viseslava 1, Belgrade, Serbia

[2] University of Novi Sad, Faculty of Technical Sciences, Trg Dositeja Obradovica 6, Novi Sad, Serbia

[3] Institute of Technical Sciences of SASA, Knez Mihailova 35, Belgrade, Serbia

Published online: 25 November 2016

Nanostructured materials are known to exhibit enhanced dielectric properties and studies of the effect of elevated temperature and frequency on dielectric and electric properties can offer valuable information on the conduction phenomena in nanostructured materials [14]. The standard structure of metal oxide gas sensors is a porous structure with a high surface area. Pseudbrookite has potential to be applied as a gas sensor [9, 10].

Complex dielectric and impedance properties of polycrystalline Fe_2TiO_5 in the temperature range below room temperature (150–300 K) were analyzed in [15] showing the presence of non-Debye type dielectric relaxation around 220–270 K mainly associated with polaron hopping. The grain and grain boundary contribution to the dielectric response change depend on the sample temperature. Only the grain contribution is present at temperatures below 170 K.

In this work we have studied dielectric, electric and impedance properties of Fe_2TiO_5 nanopowder obtained by a simple solid state process in the form of compacts and compared them to bulk samples (sintering temperature 900 °C, 2 h) with a polycrystalline structure. Investigations were conducted at temperatures of 300–423 K for compacts and 300–443 K for bulk samples, in a wide frequency range of 100 Hz–10 MHz. This enabled an analysis and comparison between changes of dielectric and electric properties of nanostructured and polycrystalline pseudobrookite (Fe_2TiO_5) at elevated temperatures that are of interest in view of possible sensor applications of pseudobrookite.

2 Experimental

Starting hematite α-Fe_2O_3 (Alfa Aesar, 99%, grain size 20–60 nm) and anatase-TiO_2 (Alfa Aesar. 99.7%, grain size 15 nm) nanopowders were homogenized in the molar ratio 1:1 (PSB11) and 1:1.5 (PSB115) in a planetary ball mill (Fritsch Pulversisette 5) in stainless steel bowls with stainless steel balls for 60 min. This was followed by drying at 150°C for 24 h. The resulting PSB11 and PSB115 powders were calcined in air at 900°C for 2 h and after that sieved through a 400 mesh. X-ray diffraction (XRD) analysis of was performed on a Philips PW 1050 diffractometer with CuK_α radiation, step 0.02 s and holding time 10 s. Structural refinement was performed using the Rietveld method with the GSAS package [16] with the EXPGUI graphical user interface [17]. Samples were analyzed for the presence of TiO_2 (anatase and rutile), α-Fe_2O_3 (hematite) and pseudobrookite (orthorhombic–space group *Cmcm* [18] and monoclinic space group *C*2/*c* [19]).

Scanning electron micrographs (SEM) were recorded on a TESCAN electron microscope VEGA TS 5130MM device. Transmission electron micrographs (TEM) were recorded on a JEOL JEM-1400 PLUS device.

Samples for electrical measurements were prepared by pressing compacts of powders PSB11 and PSB115 (10 mm in diameter) denoted as PSB11c and PSB115C. Compacts were coated with silver paste to obtain good ohmic contacts. AC (alternating current) parameters were measured in the frequency range 100 Hz–1 MHz on a HP-4194A impedance analyzer at room temperature and in the temperature range 323–423 K (50–150 °C). Samples were prepared in capacitor form and can be considered electrically equivalent to a capacity C_p in parallel with a resistor R_p with impedance, so admittance was calculated as:

$$\underline{Y} = \frac{1}{R_p} + j\omega C_p = G + jB \tag{1}$$

where G and B are real and imaginary parts of admittance $\underline{Y}$. Real and imaginary parts of complex permittivity (ε_r') and (ε_r'') were calculated as:

$$\underline{Y} = j\omega C_0\left(\varepsilon_r' - j\varepsilon_r''\right) = \omega\varepsilon_r'' C_0 + j\omega\varepsilon_r' C_0, \tag{2}$$

$$\varepsilon_r' = \frac{B}{\omega C_0}, \varepsilon_r'' = \frac{G}{\omega C_0}, \tag{3}$$

while AC conductivity and resistivity were calculated as:

$$\sigma_{AC} = \omega\varepsilon_0\varepsilon_r'', \ \rho_{AC} = 1/\sigma_{AC}, \tag{4}$$

where C_0 is capacitance of the corresponding air gap parallel plate capacitor with the same dimensions as the tested sample, ε_0 is the permittivity of free space of vacuum, ω is the angular frequency.

Bulk samples (PSB11b and PSB115b) were obtained by sintering pressed compacts at 900 °C for 2 h. They were also prepared for electrical measurements by coating with silver paste on both sides and measured in the same way as the compacts in the temperature range 300–443 K (room temperature −190 °C).

3 Results and discussion

3.1 Structural analysis

XRD analysis of PSB11 and PSM115 powders showed that in both cases orthorhombic pseudobrookite had formed. Besides pseudobrookite both PSB11 and PSB115 powders contained traces of hematite and rutile. The amount of rutile was slightly higher in PSB115 powder that was expected since it contained an excess amount of starting anatase. The weight ratio, lattice parameters and crystallite size determined from Rietveld analysis for both powders are also shown in Fig. 1.

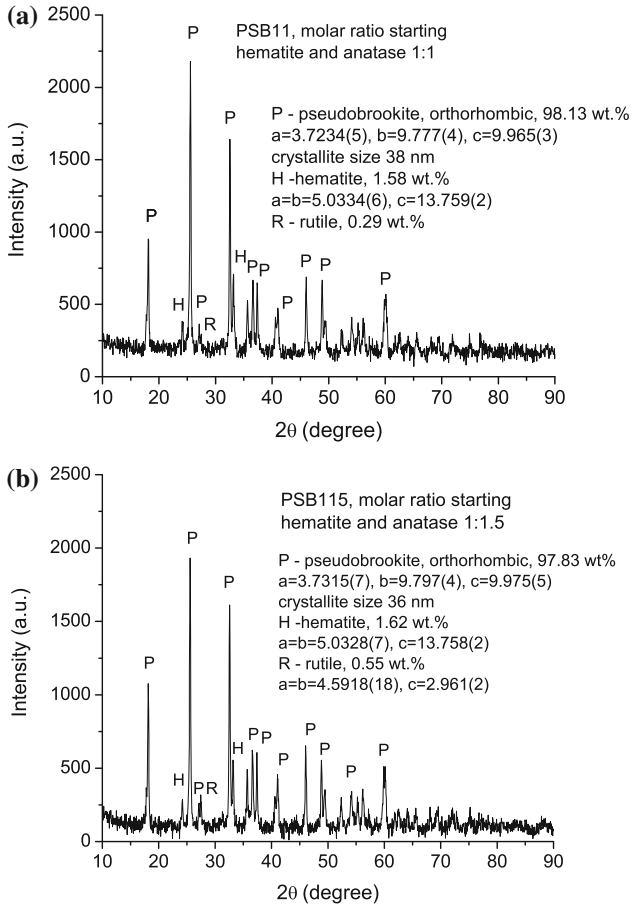

Fig. 1 XRD diffractogram of PSB11 (**a**) and PSB115 (**b**) powders, lattice parameters, weight ratio and crystallite size determined using Rietveld analysis

SEM images show that in both cases small grain size powder was obtained (PSB11-Fig. 2, PSB115-Fig. 3). TEM images showed that due to the powder synthesis process (mechanical activation combined with calcination) powder agglomeration occurred. TEM images (Figs. 2, 3) showed that in both cases powder agglomerates consisting of small agglomerated grains were also surrounded by very small powder particles. The size of the small particles was between 5–8 nm for PSB11 and 3–6 nm for PSB115 showing that excess TiO_2 resulted in a slightly smaller particle size.

3.2 Dielectric constant and loss tangent

The frequency dependence of the dielectric constant (real part of dielectric permittivity, ε_r') for all four analyzed samples at room temperature is shown in Fig. 4. The values of the dielectric constant decreased with the increase in frequency for all analyzed pseudobrookite samples. In the case of compacts similar values were obtained for both sample compositions (the slight difference between the change in dielectric constant with frequency at room temperature for PSB11c and PSB115c samples is shown as an inset in Fig. 4) in the range of around 120 at 100 Hz to 15 at around 10 MHz. For both compact compositions the dielectric constant values continually decreased in the whole analyzed frequency range and increased with the increase in temperature (Fig. 4). In the case of sintered (bulk) samples, the dielectric constant values at room temperature were much higher and are comparable to the values obtained by Sharma et al. [15] also at room

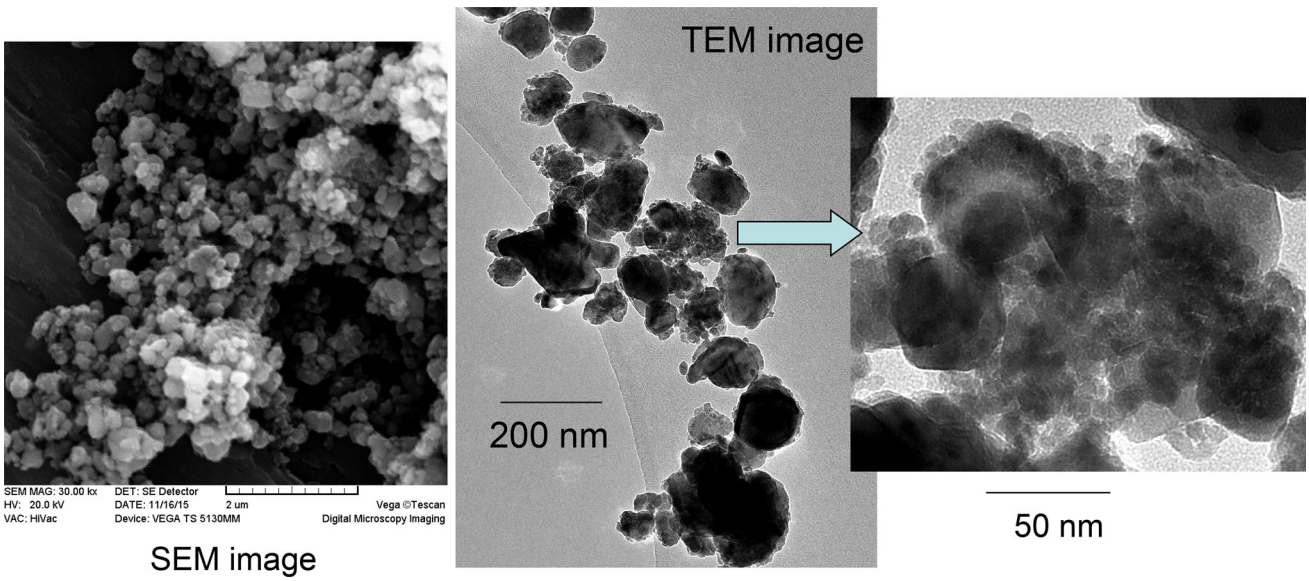

Fig. 2 SEM and TEM micrographs of PSB11 powder

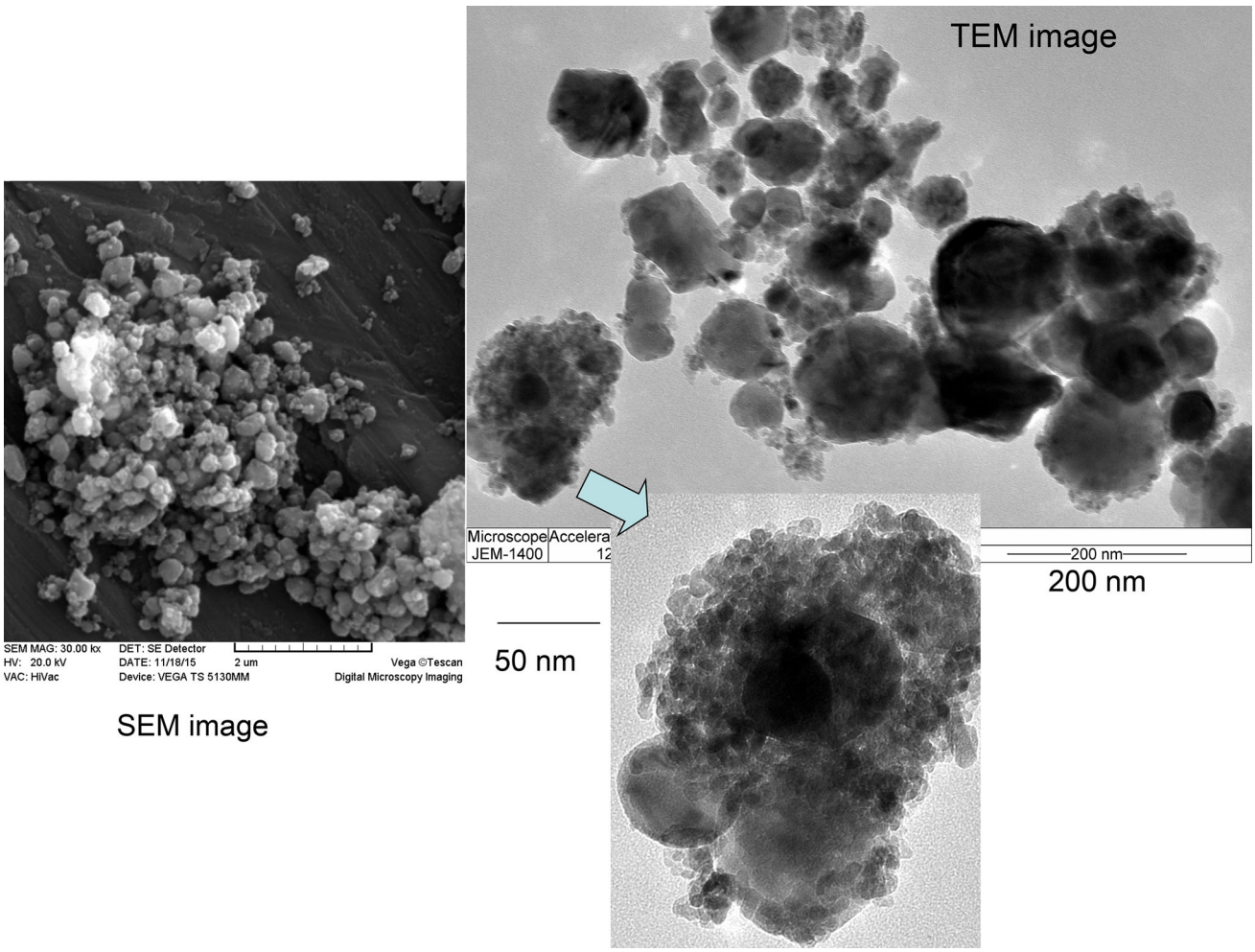

Fig. 3 SEM and TEM micrographs of PSB115 powder

temperature with high dispersion at low frequencies and values obtained by Djuric et al. [20] for bulk samples with the PSB115 composition sintered in the temperature range 1000–1250 °C. After an inflection point a slower decrease takes place at higher frequencies, and for PSB11b the dielectric constant is almost independent of frequency at higher frequencies. In the case of sintered/bulk samples difference in sample composition (excess rutile in PSB115b) results in differences in dielectric constant change with frequency. Increase in sample temperature for both PSB11 and PSB115 bulk samples shows a slower decrease at lower frequencies, with a more rapid decrease moving towards higher frequencies as the sample temperature increases. If dispersion of the dielectric constant is explained on the base of interfacial polarization due to the inhomogenous sample structure, then accumulation of charge carriers at the boundaries between conductive grain regions and highly resistive grain boundary regions is responsible for higher values at low frequencies. At higher frequencies these charges are not able to follow the field variation and their contribution to polarization is reduced [21]. According to Koop's model [22] the increase of the dielectric constant with increase in sample temperature is attributed to the increase in the number of charge carriers with increase in sample temperature leading to an enhanced build-up of space charge polarization.

The change of dielectric loss tangent with frequency at different temperatures (Fig. 5) shows that in the case of nanopowder compacts it decreases with increase in frequency with maxima at higher frequencies that shift to even higher frequencies with increasing sample temperature. A maximum in the dielectric loss tangent is noted in the case when the frequency of hopping charge carriers is approximately equal to the external field frequency [21]. The dielectric loss tangent values were slightly lower for PSB115c compared to PSB11c samples. In the case of bulk samples the dielectric loss tangent values are higher and two maxima can be noted at room temperature. Sample composition also has an influence on the position of these maxima, as they are shifted towards higher frequencies for

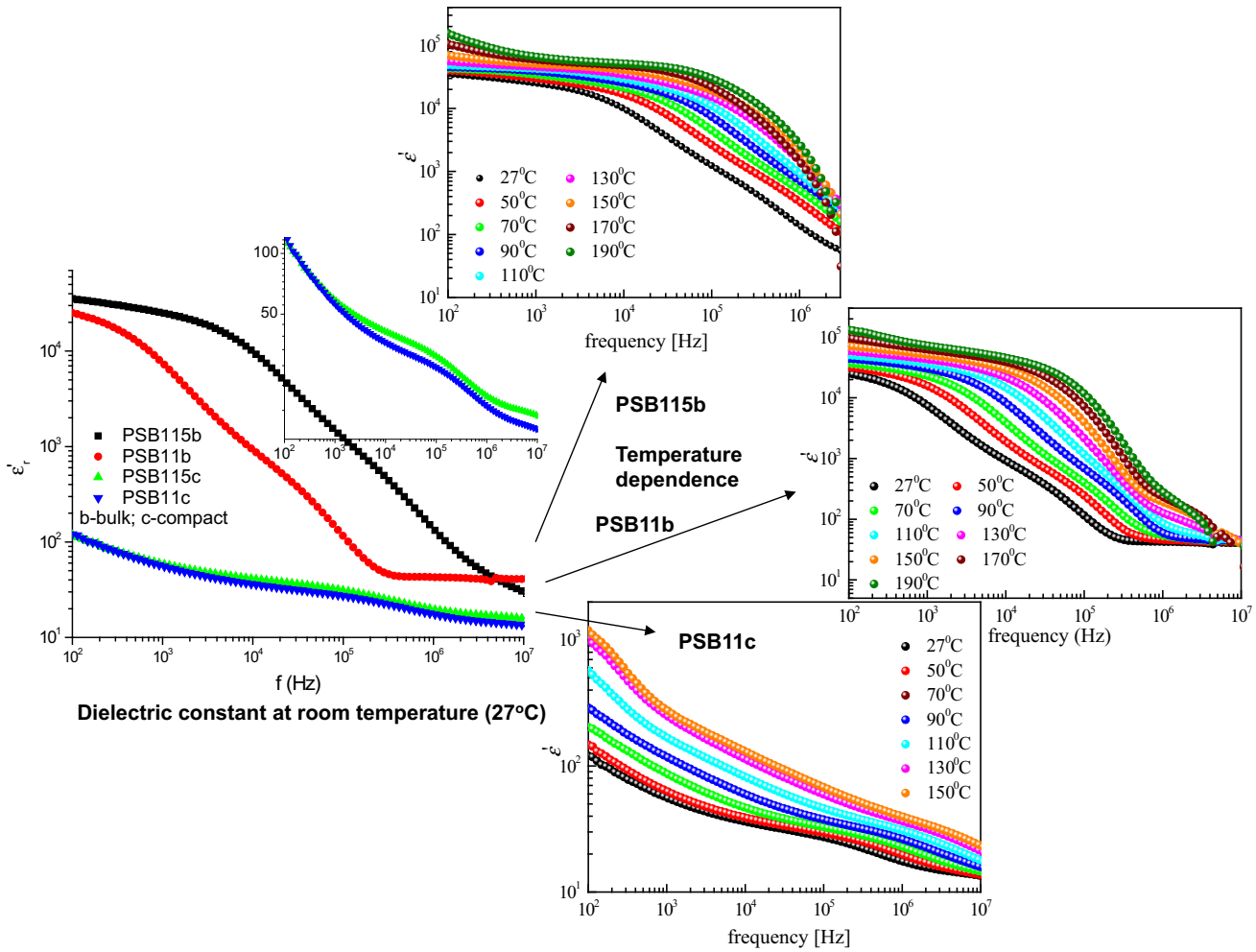

Fig. 4 Frequency dependence of the dielectric constant for PSB bulk samples and compacts

PSB115b compared to PSB11b. With increase in sample temperature above 343 K the shape of the curve changes for both PSB11 and PSB115 bulk samples, showing a decrease at low frequencies, followed by increase of the dielectric loss tangent with increase in frequency, shifting slightly with further increase with sample temperature and with no clear maxima.

3.3 Complex impedance analysis

Change in the real and imaginary part of impedance with frequency at different temperatures for PSB11 and PSB115 compacts and bulk samples does not show much difference due to sample composition (comparison between PSB11 and PSB115 samples), but there are noticeable differences between compacts and bulk/sintered samples, as shown in Figs. 6 and 7.

In the case of PSB11 and PSB115 compacts the real part of impedance (Z') decreases with frequency for both samples (PSB11 and PSB115), with the starting value decreasing with increasing sample temperature, almost merging at high frequencies (Fig. 6a). This decreasing trend of Z' confirms the negative temperature coefficient of resistance (NTCR) type behavior of this semiconducting material [23]. With rise in temperature barrier properties in the material reduce, releasing space charge that may be responsible for increase in material conductance at higher frequencies [24]. In addition, the temperature-dependent Z' shows a plateau on the low frequency side followed by a nearly negative slope on the high frequency side, indicating a crossover from low frequency relaxation behavior to high frequency dispersion phenomenon. This segment of nearly constant real impedance becomes dominant with increasing temperature, suggesting strengthened relaxation behavior [25]. In the case of sintered samples the real part of complex impedance also decreases with increase in sample frequency. Overall the values obtained for sintered samples are lower, 10–30 kΩ at 100 Hz, depending on the sample temperature, compared to several MΩ obtained for compacts. At lower temperatures (room −110 °C) the shape of

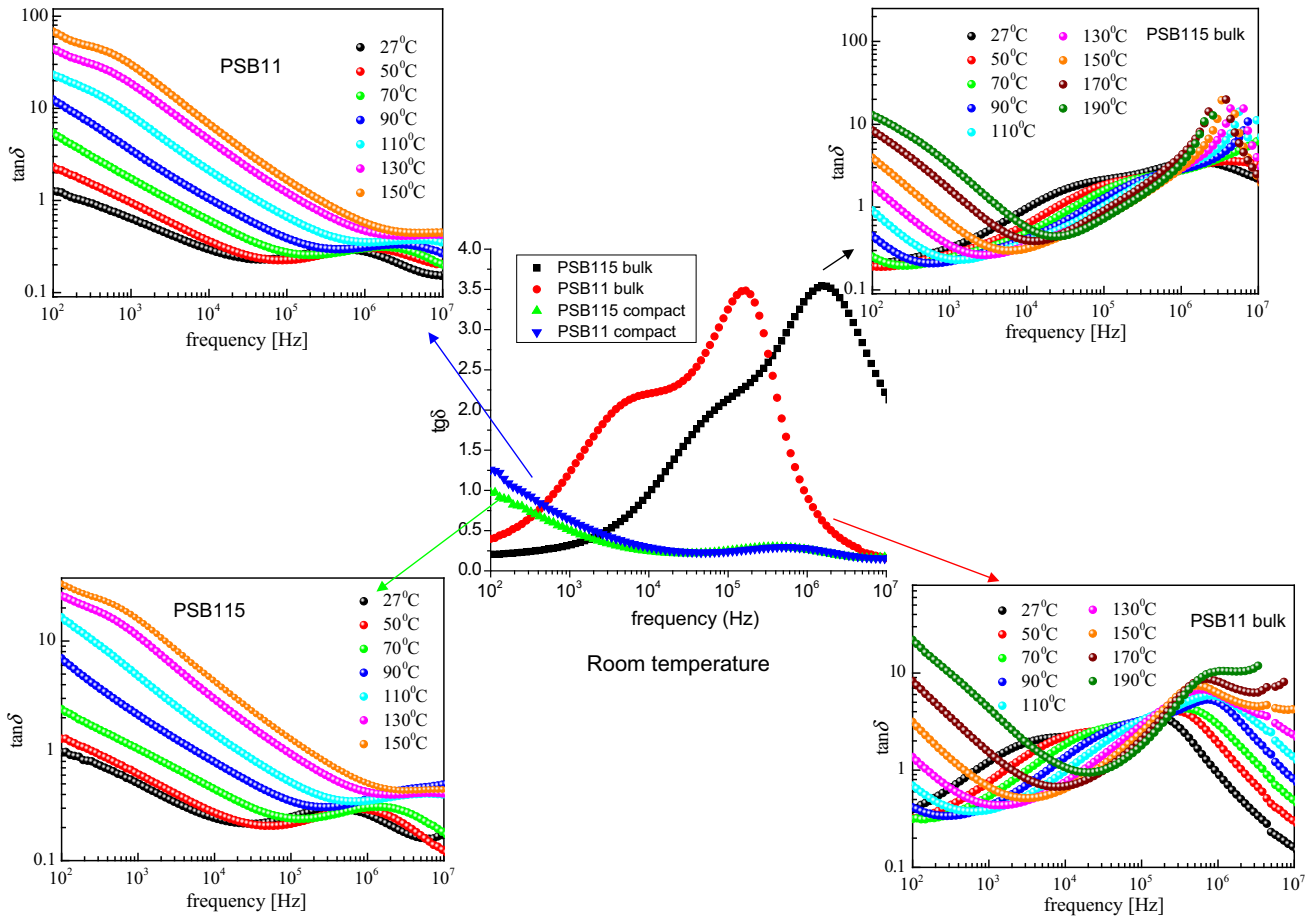

Fig. 5 Frequency dependence of the loss tangent for PSB bulk samples and compacts

the curve is different compared to compacts, with the real part of complex impedance decreasing continuously with increase in frequency. With increase in sample temperature (130–190 °C) the curve shape for bulk samples resembles the curve shape obtained for compacts showing a crossover from low frequency relaxation behavior to higher frequency relaxation behavior.

The imaginary part of impedance (Z'') of PSB115c changes shape with increase in sample temperature (Fig. 6b) showing a maximum value at temperatures above 90 °C. This maximum suggests the existence of one relaxation process, or overlapping of two relaxation processes, shifting to higher frequencies with increase in sample temperature. The relaxation peaks are due to the existence of space charge relaxation [24]. In both PSB11 and PSB115 compacts (Fig. 6b), these peaks shift towards higher frequency possibly due to an increase in the rate of hopping of charge carriers with the rise of temperature. The shifting of peaks in Z'' also indicates decreasing relaxation time of mobile charge carriers with the increase of temperature [26]. A lower relaxation time implies faster movement of mobile carriers and vice versa. Also, it is evident that the magnitude of Z'' maxima decreases with increase in temperature, indicating increasing loss in the resistive property of prepared samples [27]. In the case of sintered samples the imaginary part of complex impedance for both sample compositions (PSB11b and PSB115b) changes with frequency in a similar way to compacts, starting to show a maximum at sample temperature of 130° that shifts to higher frequencies with increase in sample temperature. Overall values obtained for sintered samples are lower than values obtained for compacts and the maxima are at lower frequencies for sintered samples though at higher sample temperatures.

Complex impedance spectra of PSB11 and PSB115 compacts and bulk samples (Figs. 8, 9) change with increase in sample temperature. In the case of compacts at room temperature (for PSB11c and PSB115c, Fig. 8) we can observe one semicircular arc. This shows that either one relaxation mechanism is dominant or the impedance response from grains and grain boundaries overlap one another. According to Batoo et al. [28] this overlapping is significant if the time constants of the different processes differ by a factor less than 100. With increase in sample

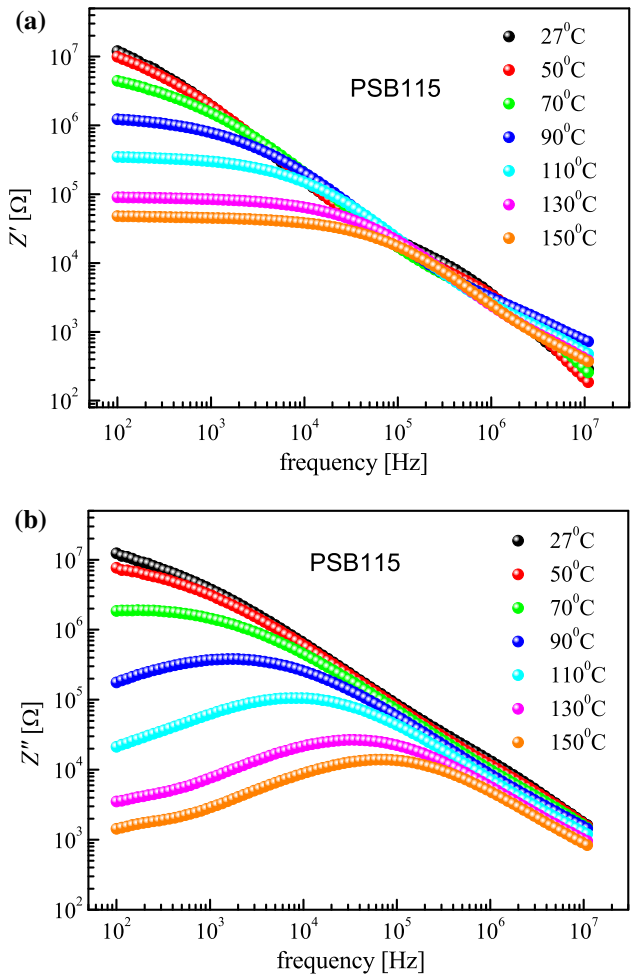

Fig. 6 Frequency dependence of the real (**a**) and imaginary part (**b**) of impedance for PSB115 compacts

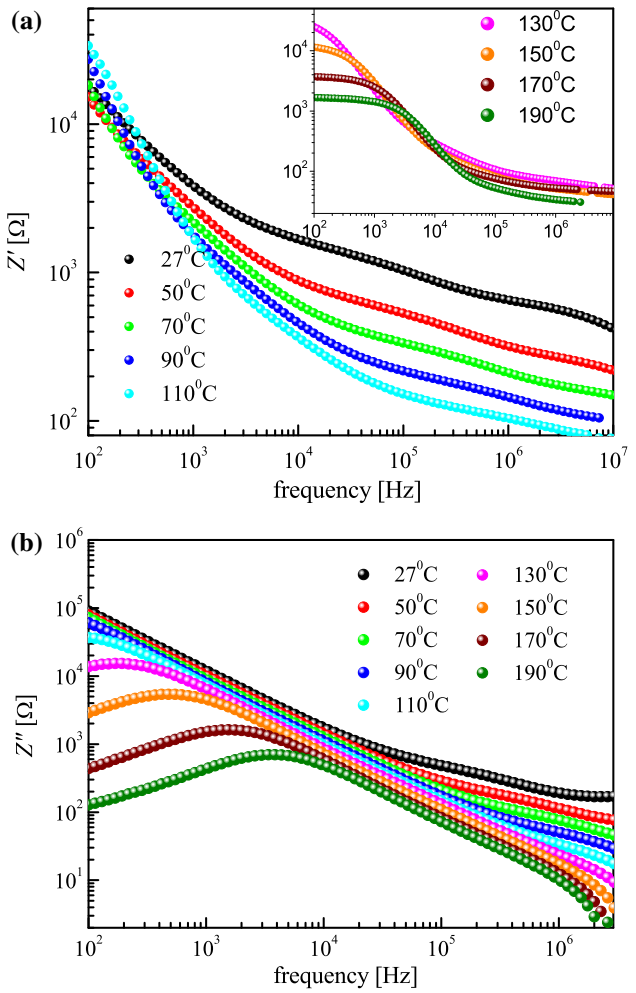

Fig. 7 Frequency dependence of the real (**a**) and imaginary part (**b**) of impedance for PSB115 bulk samples

temperature the complex impedance values decrease and a semicircle appears with a diameter that varies with temperature. This means that the temperature-dependent impedance (spectra) support the increase in conductivity and decrease in relaxation time [29]. Also, such behavior suggests that PSB11c and PSB115c possess a negative temperature coefficient of resistance, implying a thermally activated conductivity of these materials [23]. Impedance data was successfully analyzed with an equivalent circuit consisting of a serial connection of parallel grain and grain boundary resistance and capacitance (Fig. 8). Taking into account the observed non–ideal Debye type behavior of prepared samples, a constant phase element (CPE) was used to replace the capacitor as the semicircle was depressed. The real value of capacitance was determined as:

$$C_{CPE} = (A \cdot R^{-(n-1)})^{1/n}, \quad (5)$$

where R, A and n are resistance and CPE parameter values determined from the applied model, respectively, as described in detail in [30]. Analysis and simulation of impedance spectra was performed using EIS Spectrum Analyzer software [31]. The values of the equivalent circuit parameters were determined with a fitting error of about 2%.

In the case of sintered (bulk) samples the complex impedance spectra shows part of a semicircular arc at lower frequencies reflecting the dominant influence of grain boundaries, with a small semicircular component at high frequencies reflecting smaller influence of the grains. This is shown in detail in Fig. 9a–c, with Fig. 9a showing the complex impedance spectra for PSB115b at room temperature and 50 °C, Fig. 9b at 70 and 90 °C, with insets showing part of the spectra at high frequencies. At room temperature Sharma et al. [15] obtained a similar impedance response for polycrystalline pseudobrookite. At frequencies below 68 kHz the dielectric behavior was mainly due to grain boundary contributions, while the high frequency behavior was due to grain contributions. With

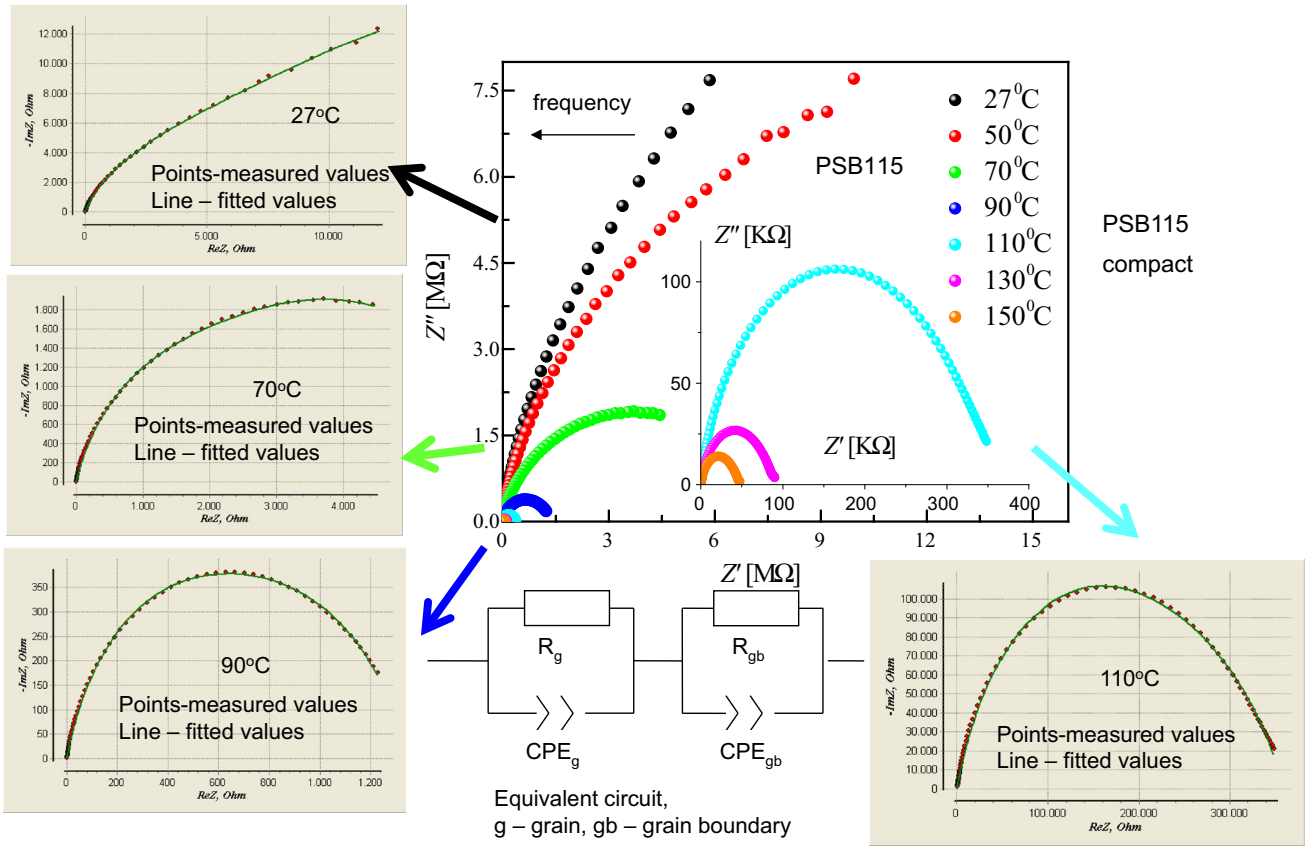

Fig. 8 Complex impedance diagrams for PSB115 compacts (*points* denote measured values, *lines* denote fitted values) and applied equivalent circuit

increase in sample temperature (Fig. 9) the impedance values decrease and the semicircular arc is a full semicircle at 170 °C. The equivalent circuit used to model the impedance of bulk PSB11 and PSB115 samples is shown in Fig. 9c and consisted of a resistance denoting the grain component serially connected with a parallel resistance and CPE element denoting the grain boundary component.

The temperature dependence of the determined grain and grain boundary resistance for compacts and grain boundary resistance for bulk samples can be analyzed using the using the adiabatic small polaron hopping (SPH) model [32],

$$R_{g,gb}/T = A_o \exp(E_a/kT) \tag{6}$$

where A_o is the pre-exponential factor, k is the Boltzmann constant and E_a is the activation energy for conduction. Figure 10 shows the dependence of the determined grain and grain boundary resistance for compacts, with the inset showing the linear dependence of ln (R/T)−1/T used to determine the activation energy. The activation energy values were determined as 0.605 and 0.571 eV for grain conduction in PSB11c and PSB115c, and 0.704 and 0.756 eV for grain boundary conduction in PSB11c and PSB115c samples, respectively. In the case of bulk samples the activation energy for grain boundary conduction was determined as 0.724 eV for PSB11b and 0.644 eV for PSB115b samples. In all cases the determined grain boundary resistance values decreased with increase in sample temperature in the range from 10^7 to 10^4 Ω.

In the case of compacts the grain and grain boundary relaxation frequency increased with increase in sample temperature, with the grain boundary relaxation frequency in the range between 10^2 and 10^5 for grain boundaries and 10^3 and 10^6 for grains for both samples. In the case of bulk samples the grain boundary relaxation frequency was between 1 and 10^4, showing that for bulk samples this process occurred at lower frequencies. The grain and grain boundary relaxation time can be expressed as [32]:

$$\tau_{g,gb} = \tau_0 \exp(E_{g,gb}/kT), \tag{7}$$

where τ_0 is the pre-exponential factor, k is the Boltzmann constant, $E_{g,gb}$ is the activation energy for the relaxation process at grains and grain boundaries and T is the temperature. The activation energy values were determined as 0.574 and 0.547 eV for grains, and 0.690 and 0.631 eV for grain boundaries for PSB11c and PSB115c samples,

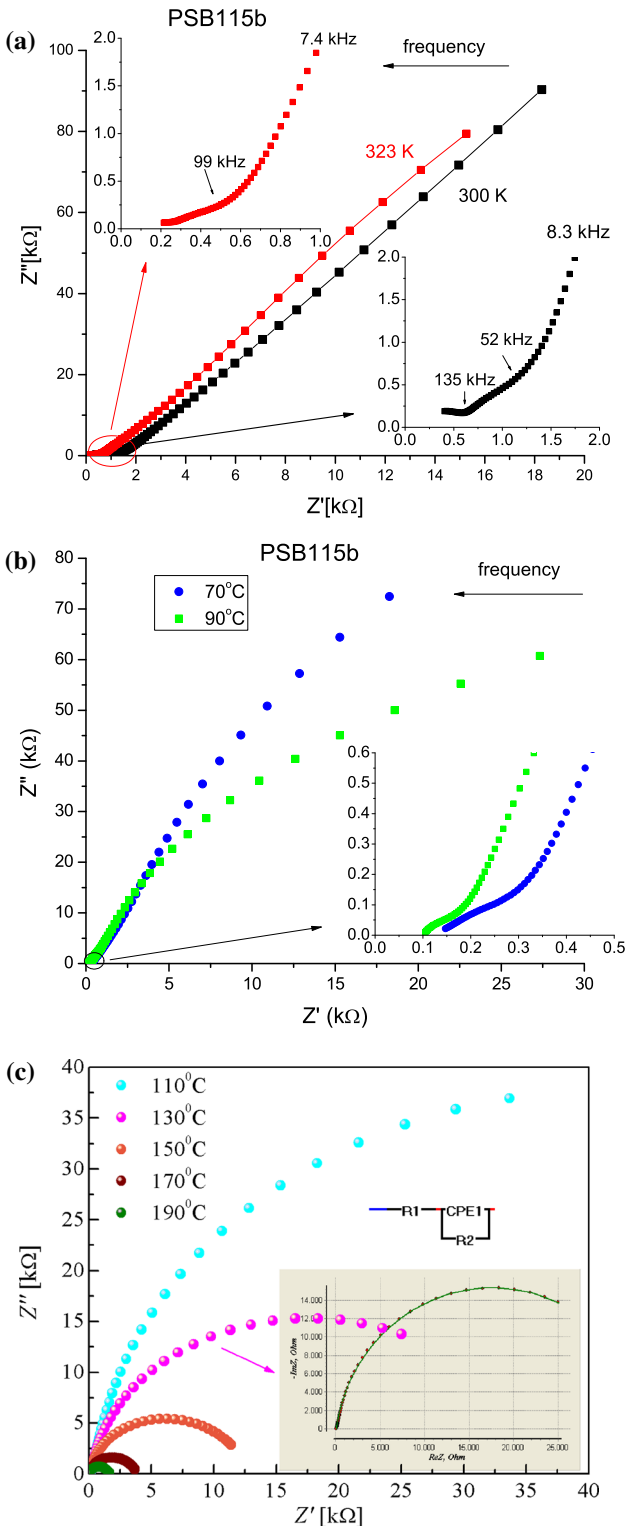

Fig. 9 Complex impedance diagrams for PSB115 bulk samples **a** at 27 and 50 °C, *insets* high frequency values, **b** at 70 and 90 °C, insets: high frequency values, **c** at 110–190 °C, *inset* example of fitted curve at 130 °C using the shown equivalent circuit

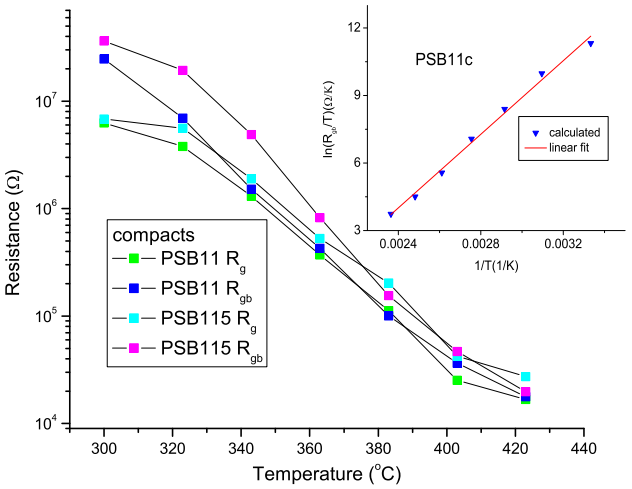

Fig. 10 Grain and grain boundary resistance determined for PSB11 and PSB115 compacts, *inset* $\ln(R_{gb}/T)-1/T$ dependence used for determining the activation energy for PSB11c

respectively. In the case of bulk samples the activation energy for relaxation at grain boundaries was determined as 0.564 eV for PSB11b and 0.645 eV for PSB115b.

Analysis of the activation energy values obtained for PSB11 and PSB115 compacts shows that the activation energy for conduction at grains (for PSB11c slightly higher than PSB115c) was lower than at grain boundaries. The activation energy for relaxation was lower at grains than at grain boundaries and slightly lower values were obtained for PSB115c compared to PSB11c. These differences are due to the differences in sample composition and are consistent with conduction induced by hopping of charge carriers, in this case electron hopping between Fe^{2+} and Fe^{3+}. In the case of bulk samples the difference in composition between PSB11b and PSB 115b resulted in slightly lower activation energy for conduction for PSB115b that also had slightly higher activation energy for relaxation.

3.4 AC conductivity

The change in *AC* conductivity was similar for the two different sample compositions (PSB11 and PSB115) but different for compacts and bulk samples as shown in Fig. 11. The values obtained for compacts were higher than for bulk samples as expected and increased with increase in frequency. For both compacts and bulk samples the sample conductivity increased with increase in sample temperature. This is due to the increase in thermally activated electron drift velocity of charge carriers according to the hopping conduction mechanism [33]. The change of

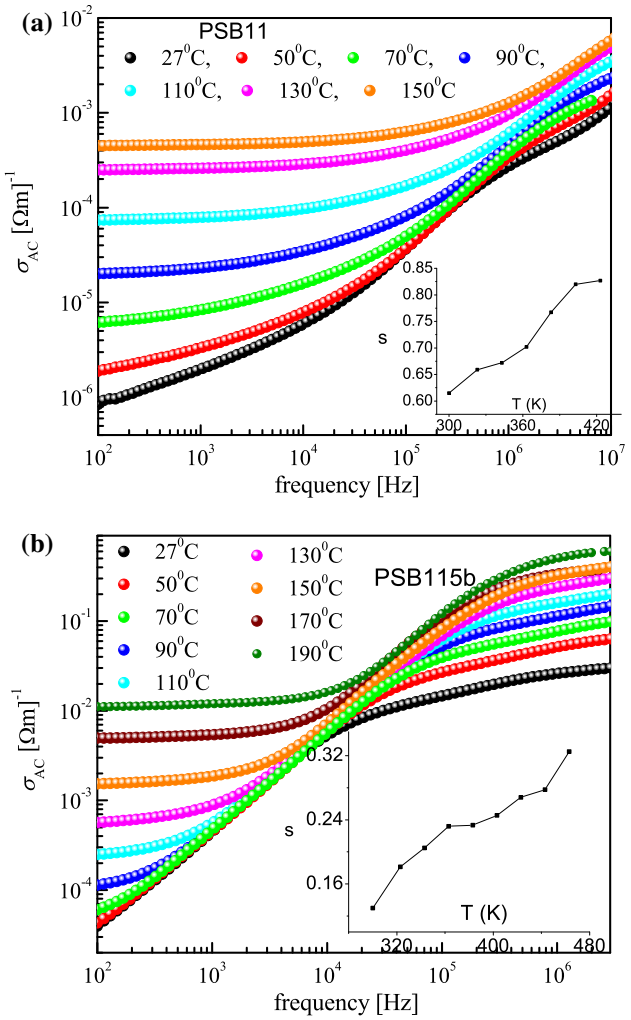

Fig. 11 Frequency dependence of electrical conductivity for **a** PSB11 compacts, *inset* variation of frequency exponent *s* with sample temperature; **b** PSB115 bulk samples, *inset* variation of frequency exponent *s* with sample temperature

conductivity with frequency can be correlated with hopping dynamics of charge carriers according to the Jonscher power law [15, 34]:

$$\sigma_{AC} = \sigma_{DC} + A\omega^{s}, \tag{8}$$

where σ_{DC} is the *dc* conductivity, A is the pre-exponential factor and and s is the frequency exponent whose value lie between 0 and 1. Insets in Fig. 11a, b show the determined dependence of the frequency exponent for compacts and bulk samples (similar values were obtained for both PSB11 and PSB115 compositions). The values obtained for the frequency exponent were between 0.61 and 0.83 for compacts and 0.12 and 0.32 for bulk samples. As the frequency exponent increases with increase in sample temperature the quantum mechanical-tunneling (QMT) model for the case of small polaron hopping can be applied to describe the conduction mechanism [33, 35].

4 Conclusion

Structural analysis revealed that orthorhombic pseudobrookite was obtained by simple solid state synthesis of starting hematite and anatase (molar ratio 1:1—PSB11 and 1:1.5—PSB115), with small amounts of excess hematite and rutile (slightly more in PSB115 due to excess starting anatase). SEM and TEM analysis showed that both powders contained agglomerates consisting of small agglomerated grains surrounded by small nanosized particles (5–8 nm for PSB11 and 3–6 nm for PSB115). The change in dielectric constant with frequency was due to space charge polarization and it increased with increase in sample temperature. Slightly lower dielectric loss was obtained for PSB115 compacts. The impedance data was analyzed using equivalent circuit models, which for compacts included the influence of grain and grain boundary components, while in bulk samples the influence of the grain boundary component was dominant. Activation energies for conduction (at grains and grain boundaries for compacts and grain boundaries for bulk samples) and activation energies for relaxation were determined showing that conduction was induced by hopping of charge carriers and reflecting the influence of sample composition. Electrical conductivity increased with increase in sample temperature and followed the Jonscher power law correlating hopping dynamics of charge carriers with increase in frequency. Increase in sample temperature resulted in increase of the determined frequency exponent for both compacts and bulk samples indicating that the quantum mechanical-tunneling model for the case of small polaron hopping can be applied in the analyzed temperature range.

Acknowledgements The authors would like to express their gratitude to Dr. M. Mitric for XRD measurements and Dr. N. Labus for help with TEM sample preparation. This work was performed as part of projects III45007 and III45014 financed by the Ministry for Education, Science and Technological Development of the Republic of Serbia.

References

1. Q. Liu, J. He, T. Yao, Z. Sun, W. Cheng, S. He, Y. Xie, Y. Peng, H. Cheng, Y. Sun, Y. Jiang, F. Hu, Z. Xie, W. Yan, Z. Pan, Z. Wu, S. Wei, Nat. Commun. **5**, 5122 (2014)
2. Z. Lou, Y. Li, H. Song, Z. Ye, L. Zhu, RSC Adv. **6**, 45343 (2016)
3. M. Ramezani, A. Davoodi, A. Malekizad, S.M. Hosseinpour-Mashkani, J. Mater. Sci.: Mater. Electron **26**, 3597–3962 (2015)
4. P.S. Bassi, S.Y. Chiam, G.J. Barber, L.H. Wong, ACS Appl. Mater. Interfaces **6**, 22490 (2014)

5. P.S. Bassi, R.P. Antony, P.P. Boix, Y. Fang, J. Barber, L.H. Wong, Nano Energy **22**, 310 (2016)
6. M. Dondi, F. Matteucci, G. Cruciani, G. Gasparotto, D.M. Tobaldi, Solid State Sci. **9**, 362 (2007)
7. Y. Ku, Y.-C. Liu, P.-C. Chiu, Y.-L. Kuo, Y.-H. Tseng, Ceram. Int. **40**, 4599 (2014)
8. K.-M. Min, K.-S. Park, A.-H. Lim, J.-C. Kim, D.-W. Kim, Ceram. Int. **38**, 6009 (2012)
9. R. Yu, Z. Li, D. Wang, X. Lai, C. Xing, M. Yang, X. Xing, Scripta Mater. **63**, 155 (2010)
10. Z.Z. Vasiljevic, M.D. Lukovic, M.V. Nikolic, N.B. Tasic, M. Mitric, O.S. Aleksic, Ceram. Int. **41**, 6889 (2015)
11. U. Atzimony, E. Gurewitz, M. Melamud, H. Pinto, H. Shaked, G. Gorodetsky, E. Hermon, R.M. Hornreich, S. Shtrikman, B. Wanklyn, Phys. Rev. Lett. **43**, 782 (1979)
12. J.L. Tholence, Y. Yashurin, J.K. Kjems, B. Wanklyn, J. Magn. Magn. Mater. **54–57**, 203 (1986)
13. S. Sharma, T. Basu, A. Shahee, K. Singh, N.P. Lalla, E.V. Sampathkumaran, Phys. Rev. B **90**, 144426 (1986)
14. N.J. Tharayil, R. Raveendran, A.V. Vaidyan, P.G. Chithra, Indian J. Eng. Mater. Sci. **15**, 489 (2008)
15. S. Sharma, T. Basu, A. Shahee, K. Singh, N.P. Lalla, J. Alloy. Compd. **663**, 289 (2016)
16. A. C. Larson, R. B. Von Dreele, General Structure Analysis System (GSAS) Los Alamos National Laboratory Report LAUR, 86–748, 2004
17. B.H. Toby, EXPGUI. J. Appl. Crystallogr. **34**, 210 (2001)
18. P. Tiedemann, H. Mueller-Buschbaum, Z. Anorg. Allg. Chem. **494**, 98 (1982)
19. M. Drofenik, L. Golic, D. Hanzel, V. Krasevac, A. Prodan, M. Bakker, D. Kolar, J. Solid State Chem. **40**, 35 (1981)
20. Z.Z. Djuric, O.S. Aleksic, M.V. Nikolic, N. Labus, M. Radovanovic, M.D. Lukovic, Ceram. Int. **40**, 15131 (2014)
21. S.F. Mansour, M.A. Elkestawy, Ceram. Int. **37**, 1175 (2011)
22. C.G. Koops, Phys. Rev. **83**, 121 (1951)
23. P. Kour, P. Kumar, S.K. Sinha, M. Kar, J. Mater. Sci.: Mater. Electron **26**, 1304 (2015)
24. S. Hcini, E. Oumezzine, M. Baazaoui, H. Rahmouni, Appl. Phys. A **120**, 1453 (2015)
25. W. Chen, W. Zhu, O.K. Tan, X.F. Chen, J. Appl. Phys. **108**, 034101 (2010)
26. R. Martínez, A. Kumar, R. Palai, J.F. Scott, R.S. Katiyar, J. Phys. D Appl. Phys. **44**, 105302 (2011)
27. S. Dutta, R.N.P. Choudhary, P.K. Sinha, A.K. Thakur, J. Appl. Phys. **96**, 1607 (2004)
28. K.M. Batoo, M.-S. Abd, El-sadek. J. Alloy. Compd. **566**, 112 (2013)
29. D.L. Sekulic, Z.Z. Lazarevic, C.D. Jovalekic, A.N. Milutinovic, N.Z. Romcevic, Sci. Sinter. **48**, 17 (2016)
30. M.V. Nikolic, D.L. Sekulic, N. Nikolic, M.P. Slankamenac, O.S. Aleksic, H. Danninger, E. Halwax, V.B. Pavlovic, P.M. Nikolic, Sci. Sinter. **45**, 281 (2013)
31. A. S. Bondarenko, G. Ragoisha, EIS Spectrum Analyzer, http://www.abc.chemistry.bsu.by
32. M. Idrees, M. Nadeem, M.M. Hassan, J. Phys. D Appl. Phys. **43**, 155401 (2010)
33. M.M. El-Nahass, A.A. Attia, G.F. Salem, H.A.M. Ali, M.I. Ismail, Phys. B **434**, 89 (2014)
34. A.K. Jonscher, Nature **267**, 673 (1977)
35. A. Ghosh, Phys. Rev. B **41**, 1479 (1990)